

Cite this article as: Zheng Yi, Bian Liping, Ji Hongliang, et al. Influence of Ca and Mn on Microstructure, Mechanical Properties, and Electrical Conductivity of As-Cast and Heat-Treated Al-Mg-Si Alloys[J]. Rare Metal Materials and Engineering, 2022, 51(11): 4010-4020.

ARTICLE

# Influence of Ca and Mn on Microstructure, Mechanical Properties, and Electrical Conductivity of As-Cast and Heat-Treated Al-Mg-Si Alloys

Zheng Yi<sup>1</sup>, Bian Liping<sup>1,2,3</sup>, Ji Hongliang<sup>1</sup>, Liu Xianwen<sup>1</sup>, Tian Feng<sup>1</sup>

<sup>1</sup> College of Materials Science and Engineering, Taiyuan University of Technology, Taiyuan 030024, China; <sup>2</sup> Shanxi Key Laboratory of Advanced Magnesium-Based Materials, Taiyuan University of Technology, Taiyuan 030024, China; <sup>3</sup> Engineering Research Center of Advanced Metal Composites Forming Technology and Equipment, Ministry of Education, Taiyuan University of Technology, Taiyuan 030024, China

**Abstract:** The Al-0.59Mg-0.54Si- $X$  ( $X=0, 0.253\text{Ca}, 0.253\text{Mn}$ ) alloys were prepared to investigate the effect of minor addition of Ca and Mn on the microstructure, mechanical properties, and electrical conductivity of the Al-0.59Mg-0.54Si- $X$  alloys after casting, solid-solution, and aging treatments. Results show that the Ca and Mn addition can significantly refine the grains of  $\alpha$ -Al matrix. Moreover, Ca can induce the precipitation of  $\text{Mg}_2\text{Si}$  and  $\text{Al}_2\text{Ca}$  particles with high contents in the as-cast  $\alpha$ -Al grains, which contributes to the optimum mechanical properties of alloys. The solid-solution and aging treatments cause the coarsening of particles and the particle segregation at the grain boundaries, leading to the rapid decline in mechanical properties but an extraordinary increase in electrical conductivity (52.44%IACS) for the alloys. Mn addition can transform the coarse  $\beta$ - $\text{Al}_3\text{FeSi}$  impurity phase at the grain boundaries into the  $\alpha$ -Al(FeMn)Si particles and also induce the precipitation of  $\text{Mg}_2\text{Si}$  and AlMn particles in the as-cast alloys. Consequently, the Al-0.59Mg-0.54Si-0.253Mn alloy after solid-solution and aging treatment exhibits the optimal mechanical properties and acceptable electrical conductivity.

**Key words:** Al-Mg-Si alloy; alloying element; mechanical properties; electrical conductivity

The Al-Mg-Si alloys with light mass, excellent electrical conductivity, and moderate strength are commonly used for overhead power lines and in other electrical engineering fields<sup>[1-3]</sup>. However, the excellent strength and the superb electrical conductivity of Al-Mg-Si alloy conductor are mutually contradictory: the higher strength is usually accompanied by the lower electrical conductivity and vice versa. Therefore, the high-strength and high-conductivity of aluminum alloys have been the research hotspot in recent decades. Alloying is an important method to excavate the alloy potential and to improve the properties of alloys for advanced research and development<sup>[4]</sup>. Besides, the alloying method and heat treatment are commonly used to enhance the strength and electrical conductivity of as-cast Al alloys. The electrical conductivity of as-cast Al- $x$ Ce alloys is generally

higher than that of the as-cast Al- $x$ La alloys ( $x=0.075\sim 1.000$ ) due to the strong purification of Fe and Si impurities in the aluminum matrix; whereas the two kinds of alloys have the similar electrical conductivity after heat treatment at 300 °C for 24 h due to the precipitation of solid solution atoms. The as-cast Al-0.15wt% Ce alloy exhibits a high electrical conductivity of 63.62%IACS with the inferior tensile strength of less than 60 MPa<sup>[5]</sup>. The as-cast Al-7Si alloys after Ti-assisted boron treatment and Al-3B-5Sr treatment have the electrical conductivity of 46.2%IACS and tensile strength of 185 MPa<sup>[6]</sup>. Zhao et al<sup>[7]</sup> reported that the electrical conductivity and the strength of as-cast Al-0.5Mg-0.35Si-0.2Fe alloy after solution treatment at 510 °C for 2 h are 51.7%IACS and 102 MPa, respectively; the electrical conductivity and the strength of as-cast Al-0.5Mg-0.35Si-

Received date: March 06, 2022

Foundation item: National Natural Science Foundation of China (52175355); National Key Research and Development Program (2018YFA0707304); Shanxi Provincial Key Research and Development Program (201903D121087)

Corresponding author: Bian Liping, Ph. D., Professor, Shanxi Key Laboratory of Advanced Magnesium-Based Materials, Taiyuan University of Technology, Taiyuan 030024, P. R. China, Tel: 0086-351-6018398, E-mail: bianliping@tyut.edu.cn

Copyright © 2022, Northwest Institute for Nonferrous Metal Research. Published by Science Press. All rights reserved.

0.2Fe alloy after aging treatment at 175 °C for 10 h are 54.5%IACS and 180 MPa, respectively.

Calcium, as an active alkaline earth metal, has low density and cost. The Ca addition can effectively refine the  $\alpha$ -Mg grains and significantly improve the high temperature strength and creep resistance of Mg alloys due to the formation of high-melting point phases,  $\text{Al}_2\text{Ca}$  and  $(\text{Mg}, \text{Al})_2\text{Ca}$ <sup>[8-10]</sup>. The solidification path and the eutectic intermetallic phases in Al-Mg-Si ternary alloys have been widely investigated<sup>[11]</sup>. However, the effect of Ca addition in aluminum alloys is still obscure. Therefore, in this research, the Al-Mg-Si alloy was used as the raw material to prepare Ca-containing Al alloys. According to the inheritance theory of microstructure, the addition of the fine-grained Mg-Al-Si eutectic alloy may refine the grain of aluminum matrix and induce fine precipitates into the as-cast Al-Mg-Si alloys. It is reported that the average secondary dendrite arm spacing (SDAS) of  $\alpha$ -Al in Al-based alloy billets after horizontal continuous casting is decreased from 170  $\mu\text{m}$  to 40  $\mu\text{m}$  with the addition of 30wt% fine-grained Al-12Si alloy<sup>[12]</sup>. However, the excessive Ca addition can hardly affect the electrical conductivity of Al alloys, because Ca has negligible solubility in the aluminum matrix. It is known that the electrical resistivity of Al can be increased by 1.02  $\mu\Omega\cdot\text{cm}$  for every increase of 1wt% Si in the solution<sup>[13]</sup>. Besides, increasing the Si content can decrease the electrical conductivity of Al-Si alloy<sup>[14]</sup>. Thus, the Ca addition can increase the electrical conductivity of Al-Mg-Si alloys by the formation of  $\text{CaSi}_2$  phase, which thereby reduces the Si solubility in the solid solution. Moreover, the iron, as the primary impurity element in Al alloys, dramatically decreases the electrical conductivity and the strength of Al alloys owing to the coarse Fe-containing intermetallic compound inclusions<sup>[15,16]</sup>. The electrical resistivity is averagely increased by 2.56  $\mu\Omega\cdot\text{cm}$  for every increase of 1wt% Fe in the solution. Mn is often added into the Al alloys to eliminate the Fe detriments. Wang et al<sup>[17]</sup> reported that the addition of 0.36wt% Mn in 6061 cast-rolled plate can transform the acicular  $\beta$ - $\text{Al}_3\text{FeSi}$  phase into the granular  $\alpha$ - $\text{Al}_{12}(\text{FeMn})_3\text{Si}$  phase, and increase the tensile strength, yield strength, and elongation of Al alloys to 195.93 MPa, 170.36 MPa, and 17.96%, respectively. However, the Mn element can significantly degrade the electrical conductivity of Al alloys due to the large solid solubility of Mn in Al matrix. It is reported that the complete dissolution of Mn and Zr in Al alloys provides a low electrical conductivity of 14.8%IACS for the as-cast Al-3.3Cu-2.5Mn-0.5Zr alloy<sup>[18]</sup>.

In this research, the Mg-10Al-27Ca eutectic master alloy and Al-20Mn master alloy were added into the Al-Mg-Si alloy to investigate the effects of Ca and Mn addition on the microstructure, mechanical properties, and electrical conductivity of the as-cast Al-Mg-Si alloys before and after heat treatment.

## 1 Experiment

The commercially pure aluminum (99.7%), commercially pure magnesium (99.9%), and Al-12Si, Al-20Mn, and Mg-

10Al-27Ca master alloys were used in this experiment. The Mg-10Al-27Ca master alloy was prepared by the smelting of the commercially pure aluminum with Mg-30Ca master alloy in a resistance furnace. Then, the prepared Mg-10Al-27Ca master alloy was cast in a copper mold of 10 mm  $\times$  10 mm  $\times$  80 mm to obtain the fine-grain structure. Three alloys (1#, 2#, 3#) were separately prepared based on those master alloys. They were smelted in a resistance furnace at 750 °C and cast in the steel molds ( $\Phi$ 40 mm $\times$ 100 mm) by the conventional gravity casting method. The chemical composition of the used alloys is listed in Table 1.

The cast ingots were cut into the plates with the dimension of 50 mm $\times$ 20 mm $\times$ 4 mm. The plates were wrapped with Al foil, solution treated (ST) at 550 °C for 5 h in a resistance furnace, and then water-quenched to room temperature. The heating rate was 5 °C/min. The 1#, 2#, and 3# alloys after the solid-solution heat treatment were defined as ST1#, ST2#, and ST3#, respectively. Subsequently, the ST1#, ST2#, and ST3# specimens were artificially aged at 180 °C for 2 h and then cooled in air, which were defined as AA1#, AA2#, and AA3#, respectively.

The alloy microstructures were characterized by optical microscope (OM), scanning electron microscope (SEM) equipped with energy disperse spectroscopy (EDS), and transmission electron microscope (TEM). The specimens were polished by HPY-1 polishing machine and etched by Keller's reagent (1vol% HF+1.5vol% HCl+2.5vol% HNO<sub>3</sub>+95vol% H<sub>2</sub>O). The thin foils for TEM observation were prepared by the double jet electropolishing in 5vol% perchloric acid+95vol% ethanol solution at -25 °C. The constituent phases were identified by the X-ray diffraction (XRD). The Vickers hardness measurements with the load of 100 g and holding time of 15 s were conducted by HVS-1000 microhardness tester. The average hardness was determined by at least five measurements. The tensile tests were conducted by SANS DNS100 universal tensile testing machine. The tensile rate was 0.5 mm/min. Finally, the fractured specimen was observed by SEM. The electrical conductivity was measured at room temperature by the Eddy Current Conductivity Meter Sigma 2008 B. The device was calibrated before each measurement with the reference sample. The average value of five measurements was used for accuracy.

## 2 Results

### 2.1 Microstructure of Mg-10Al-27Ca master alloy

XRD pattern in Fig. 1 reveals that the as-cast Mg-10Al-27Ca master alloy is composed of  $\alpha$ -Mg,  $(\text{Mg}, \text{Al})_2\text{Ca}$ ,  $\text{Mg}_2\text{Ca}$ , and  $\text{Al}_2\text{Ca}$  phases<sup>[19]</sup>. Fig.2 presents OM and SEM microstruc-

**Table 1 Chemical composition of alloys used in experiments (wt%)**

Alloy	Mg	Si	Ca	Mn	Al
1#	0.590	0.540	0.000	0.000	Bal.
2#	0.590	0.540	0.253	0.000	Bal.
3#	0.590	0.540	0.000	0.253	Bal.

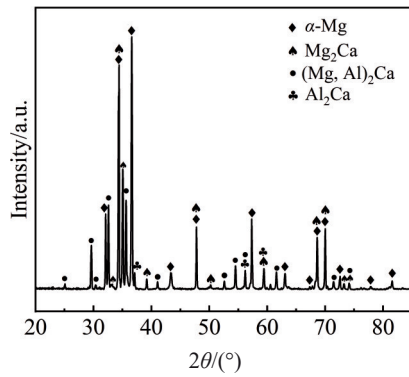


Fig.1 XRD pattern of as-cast Mg-10Al-27Ca master alloy

tures and EDS analysis results of Mg-10Al-27Ca master alloy. It can be seen that the Mg-10Al-27Ca alloy comprises abundant primary (Mg, Al)<sub>2</sub>Ca particles (point A) with the average size of 5~10 μm. Some primary (Mg, Al)<sub>2</sub>Ca particles can even grow into the ones with size of ~20 μm. In addition, a large quantity of fine lamellar eutectic structures α-Mg+Mg<sub>2</sub>Ca (point B) and a few white Al<sub>2</sub>Ca polygonal particles (point C) exist in the Mg-10Al-27Ca alloy. The Mg<sub>2</sub>Ca phase

is represented by the white stripes in Fig.2b.

## 2.2 Microstructure of as-cast alloys before and after heat treatment

XRD patterns in Fig. 3 indicate that the as-cast 1# alloy consists of α-Al, Mg<sub>2</sub>Si, and considerable β-Al<sub>3</sub>FeSi impurity phases. The minor Ca addition results in a slight decrease in the diffraction peak intensity of β-Al<sub>3</sub>FeSi phase. While the Mn addition almost eliminates the β-Al<sub>3</sub>FeSi phase and forms the new α-Al(FeMn)Si phase.

Fig. 4 shows the microstructures of as-cast 1#, 2#, and 3# alloys. The as-cast 1# alloy is composed of the coarse α-Al grains of ~200 μm, long strip-shaped β-Al<sub>3</sub>FeSi phase at grain boundaries (point A in Fig. 4j), and considerable fine Mg<sub>2</sub>Si particles. Fig. 4d~4f indicate that the α-Al grains are significantly refined to ~75 μm. A large number of fine Mg<sub>2</sub>Si, Al<sub>2</sub>Ca, and CaSi<sub>2</sub> particles are uniformly dispersed in the α-Al grains and some agglomerations along the β-Al<sub>3</sub>FeSi phase (point B in Fig. 4k) at the grain boundaries can also be observed. Fig. 4g~4i show the α-Al grains in as-cast 3# alloy are refined to ~95 μm. A large number of fine Mg<sub>2</sub>Si particles and a few Al<sub>6</sub>Mn particles are inhomogeneously distributed in the matrix, especially around the grain boundaries. As shown in Fig. 4l, the short rod-like α-Al(FeMn)Si particles indicated

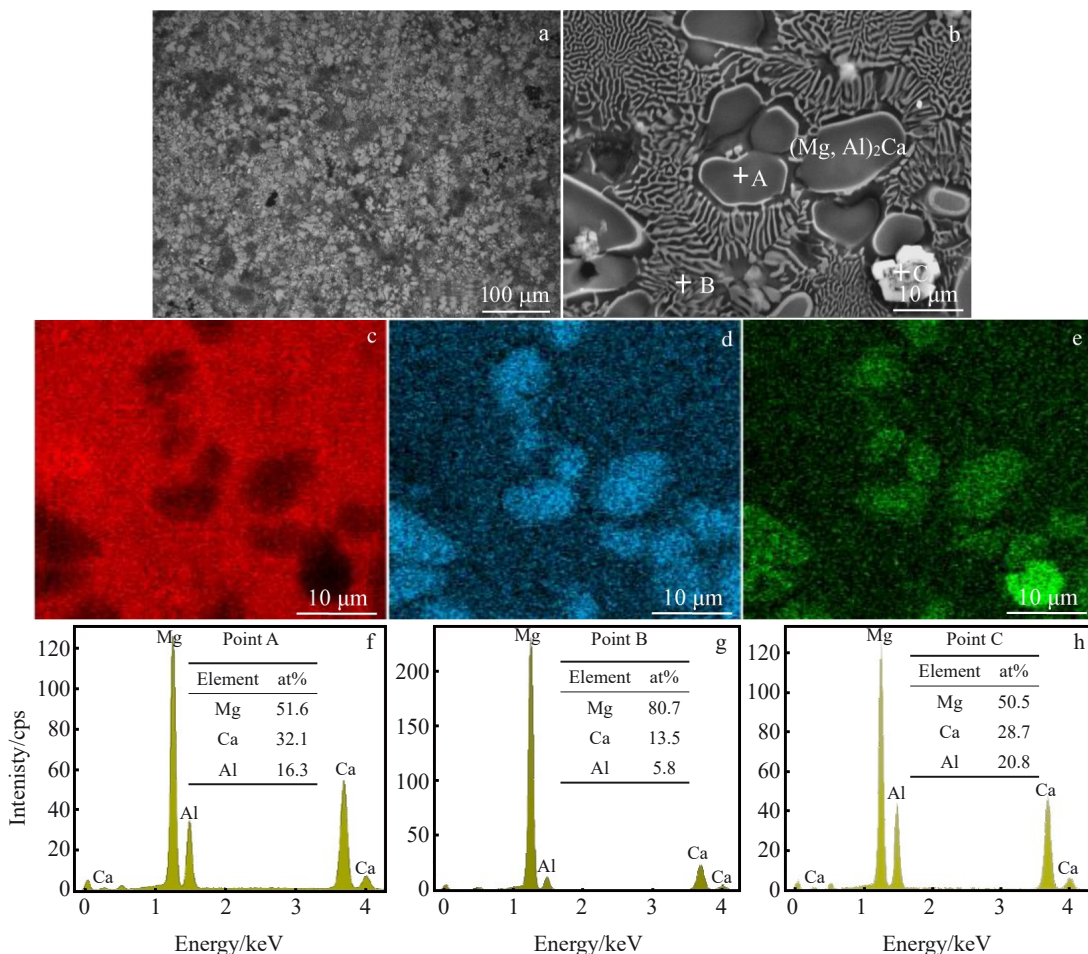


Fig.2 OM (a) and SEM (b) microstructures of as-cast Mg-10Al-27Ca master alloy; Mg (c), Ca (d), and Al (e) element distributions in as-cast Mg-10Al-27Ca master alloy corresponding to Fig.2b; EDS analysis results of point A (f), point B (g), and point C (h) in Fig.2b

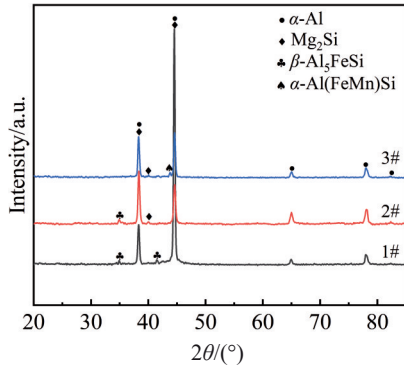


Fig.3 XRD patterns of as-cast 1#, 2#, and 3# alloys

by point C are discontinuously distributed at the grain boundaries due to the Mn addition, which causes the transformation from  $\beta$ -Al<sub>3</sub>FeSi phase to  $\alpha$ -Al(FeMn)Si phase.

TEM microstructures, EDS element distributions of as-cast 2# alloy, and the selected area electron diffraction (SAED) pattern of Mg<sub>2</sub>Si are shown in Fig.5. It is found that some Mg<sub>2</sub>Si particles of ~500 nm (indicated by white arrows in Fig.5) are agglomerated at the grain boundaries along the long strip-shaped  $\beta$ -Al<sub>3</sub>FeSi particles. Other nano-sized Mg<sub>2</sub>Si particles are clustered with the submicron Al<sub>2</sub>Ca particles in the  $\alpha$ -Al matrix.

Fig. 6 shows OM microstructures of the alloys after heat treatments. In the ST1# alloy, the long strip-shaped  $\beta$ -Al<sub>3</sub>FeSi

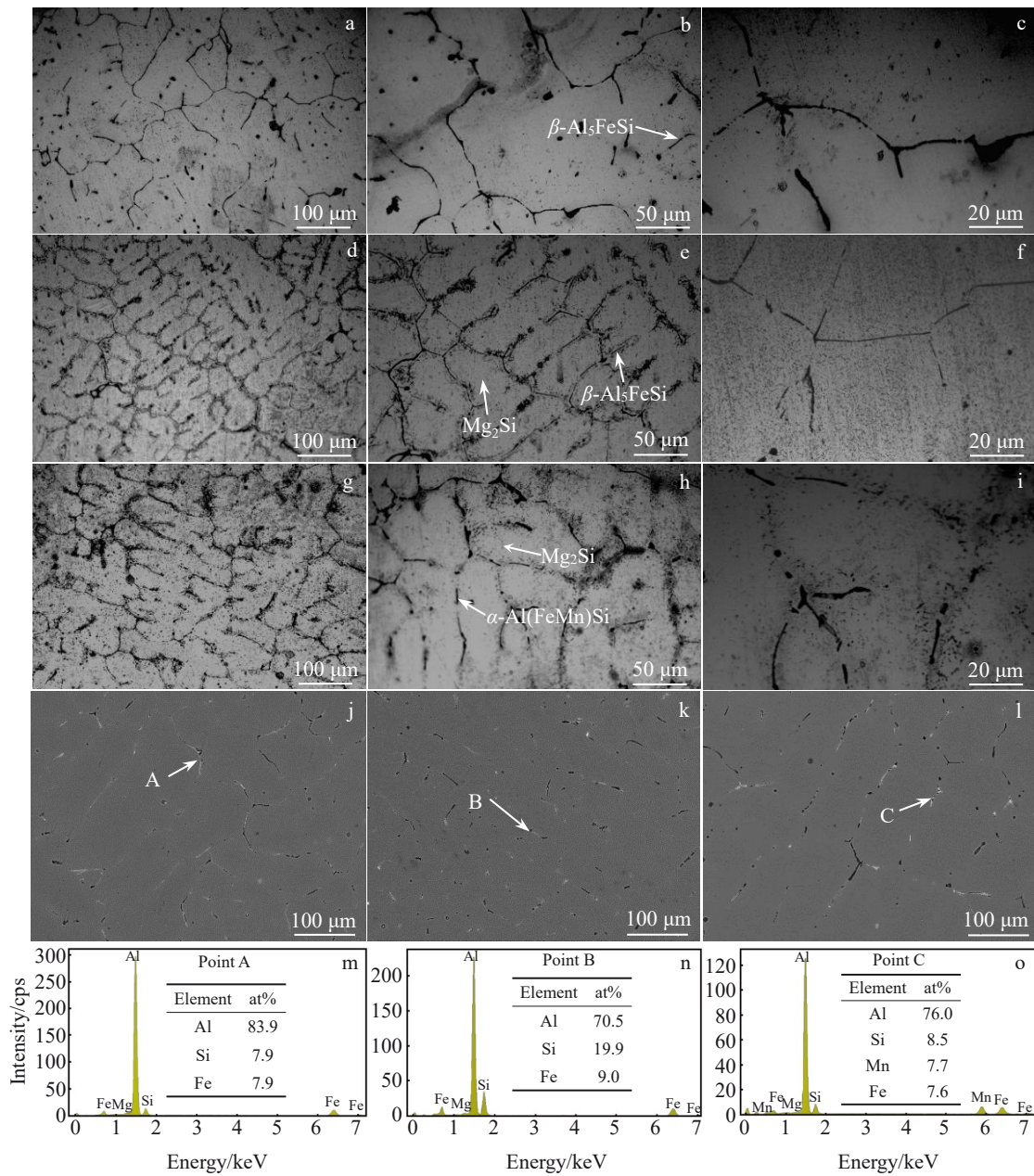


Fig.4 OM (a~i) and SEM (j~l) microstructures of as-cast 1# alloy (a~c, j), 2# alloy (d~f, k), and 3# alloy (g~i, l); EDS analysis results of point A in Fig.4j (m), point B in Fig.4k (n), and point C in Fig.4l (o)

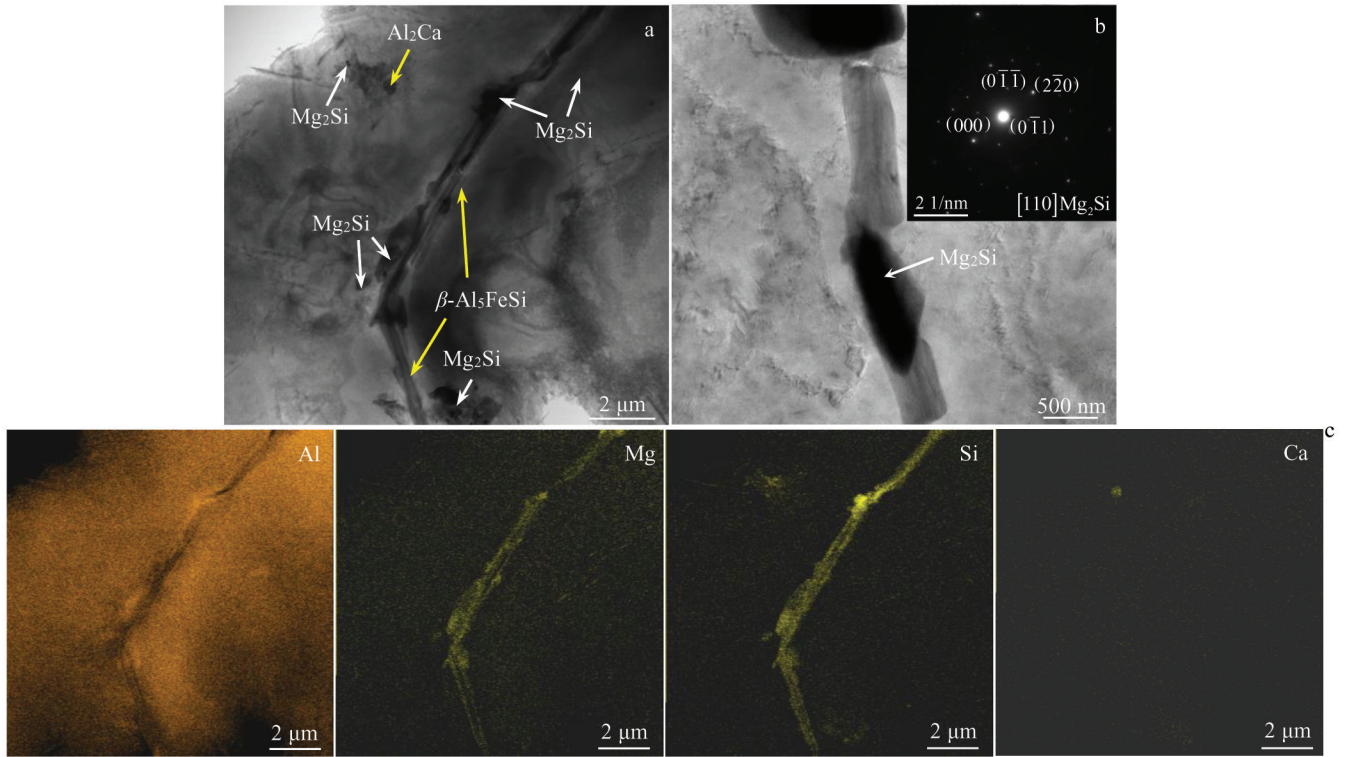


Fig.5 TEM microstructures (a) and EDS element distributions (c) of as-cast 2# alloy;  $Mg_2Si$  particles at the grain boundaries and corresponding SAED pattern (b)

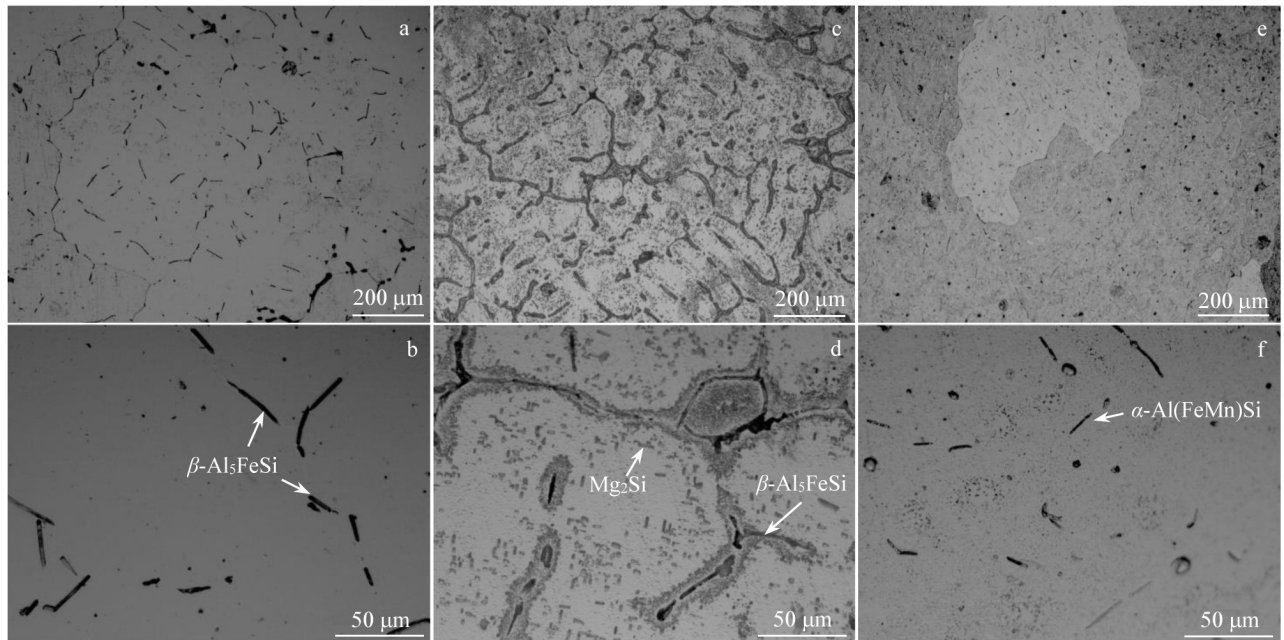


Fig.6 OM microstructures of ST1# alloy (a, b), ST2# alloy (c, d), and ST3# alloy (e, f)

particles partially dissolve and are changed into the short rods. Many  $Mg_2Si$  precipitates exist as solid solution in the alloy matrix. However, as shown in Fig.6c and 6d, the precipitates are severely coarsened into the elongated particles of 4  $\mu m$  in size and some precipitates are agglomerated around the coarse  $\beta-Al_5FeSi$  particles. The number of  $Mg_2Si$  precipitates

is slightly reduced due to the partial dissolution. A relatively uniform microstructure can be observed in the ST3# alloy. Most rod-like  $\alpha-Al(FeMn)Si$  particles dissolve and numerous fine particles form. The remanent  $\alpha-Al(FeMn)Si$  particles are about 2.5  $\mu m$  in size.

Fig. 7 and Fig. 8 show OM and SEM microstructures of

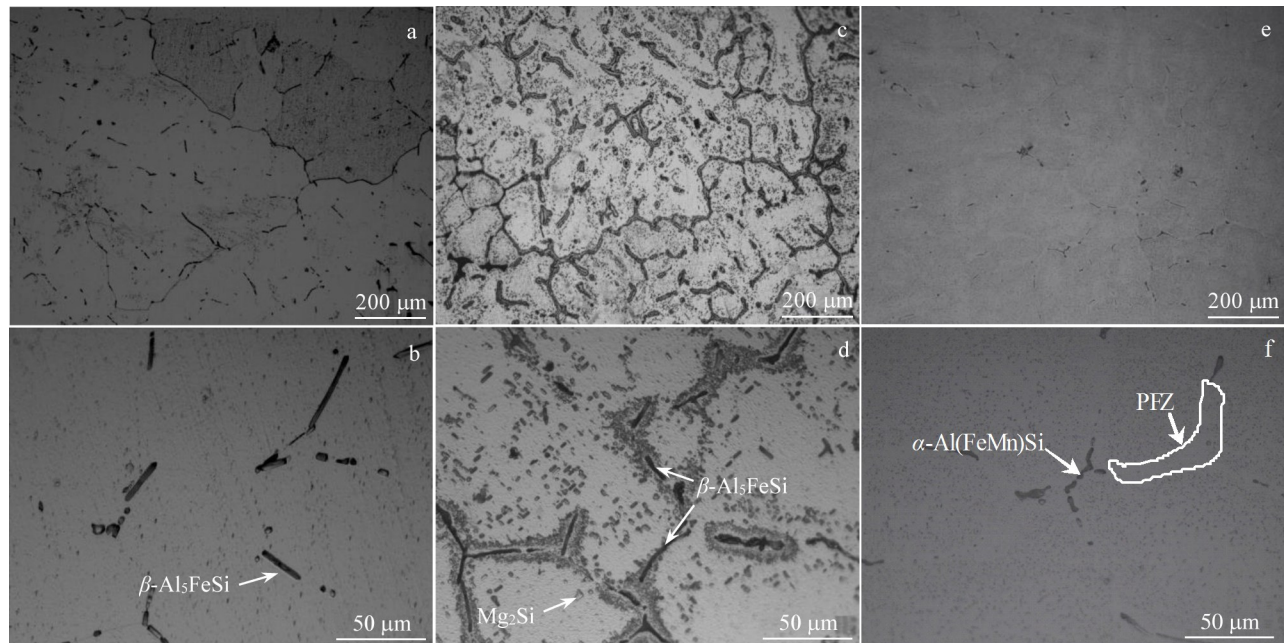


Fig.7 OM microstructures of AA1# alloy (a, b), AA2# alloy (c, d), and AA3# alloy (e, f)

AA2# alloy, respectively. Fig. 7a and 7b indicate that more fine  $Mg_2Si$  particles are precipitated in AA1# alloy during the aging treatment, but their distribution is inhomogeneous. As shown in Fig.7c and 7d, the aging treatment further aggravates the segregation of particles around the coarse  $\beta-Al_3FeSi$  particles with more precipitation of  $Mg_2Si$  particles in AA2# alloy. According to Fig. 8, the growth and agglomeration of precipitates can be observed after the solid solution and aging treatments, as well as the insoluble coarse  $CaSi_2$  intermetallic compound (point A). However, the finer and more homogeneous microstructure forms in AA3# alloy with the precipitation of numerous fine  $Mg_2Si$  particles. The precipitate free zone (PFZ) can also be observed in Fig.7f with the further dissolution of  $\alpha-Al(FeMn)Si$  particles.

### 2.3 Hardness and electrical conductivity

Fig.9 shows the measured Vickers hardness and electrical conductivity of the alloys at different states. According to Fig.9a, the hardness of 1# and 3# alloys rapidly increases after the solid solution and aging treatments. The AA3# alloy exhibits the highest hardness of 713.24 MPa. While in the as-cast condition, the 2# alloy has the highest hardness of 560.85 MPa. The heat treatment causes a dramatic decrease in the hardness of as-cast 2# alloy, and the subsequent aging treatment can only increase the hardness of ST2# alloy to a small extent. Fig.9b shows that the 1# alloy has a relatively stable electrical conductivity at as-cast, solid solution, and aging states, which is 49.7%IACS, 49.24%IACS, and 50.37%IACS, respectively. Whereas the electrical conductivity of the as-cast 2# and 3# alloys rapidly increases after the solid solution and then slightly decreases after the aging treatment: the electrical conductivity increases from 47.62%IACS to 53.78%IACS and then decreases to

52.44%IACS for the 2# alloy; the electrical conductivity increases from 38.8%IACS to 44.93%IACS and then decreases to 44.89%IACS for the 3# alloy. The maximum electrical conductivity of 53.78%IACS can be obtained for SS2# alloy.

### 2.4 Tensile properties

Fig.10 shows the tensile properties at ambient temperature of the as-cast 1#, 2#, and 3# alloys before and after aging treatments. The yield strength (YS), ultimate tensile strength (UTS), and elongation (EL) of the as-cast 2# alloy is 98 MPa, 180 MPa, and 8.3%, respectively. YS and UTS of the as-cast 2# alloy are improved, but its EL is decreased, compared with those of the as-cast 1# alloy (YS of 93 MPa, UTS of 177 MPa, and EL of 13.7%). As for the as-cast 3# alloy, compared with those of the as-cast 1# alloy, its UTS and EL decrease to 153 MPa and 8.5%, respectively; its YS increases to 99 MPa. After the solid-solution and aging treatment, the tensile properties of the as-cast 1# and 3# alloys are greatly enhanced: for the AA1# alloy, its YS is 106 MPa, UTS is 203 MPa, and EL is 23.6%; for the AA3# alloy, its YS is 110 MPa, UTS is 214 MPa, and EL is 24.9%. UTS of AA2# alloy is drastically reduced to 147 MPa, although its EL increases to 11.8%.

Fig.11 presents SEM fractographies of as-cast alloys before and after aging treatment. As shown in Fig.11a and 11b, the as-cast 1# alloy shows obvious intergranular fracture feature: the cracks are initiated and propagated mainly along the coarse  $\beta-Al_3FeSi$  impurity phase and the eutectic  $Mg_2Si$  particles at the grain boundaries. A large number of dimples can be observed in Fig. 11a. After aging treatment, the AA1# alloy exhibits an obvious ductile fracture feature with many fine dimples and significantly reduced intermetallic compound particles due to their partial dissolution during the solid

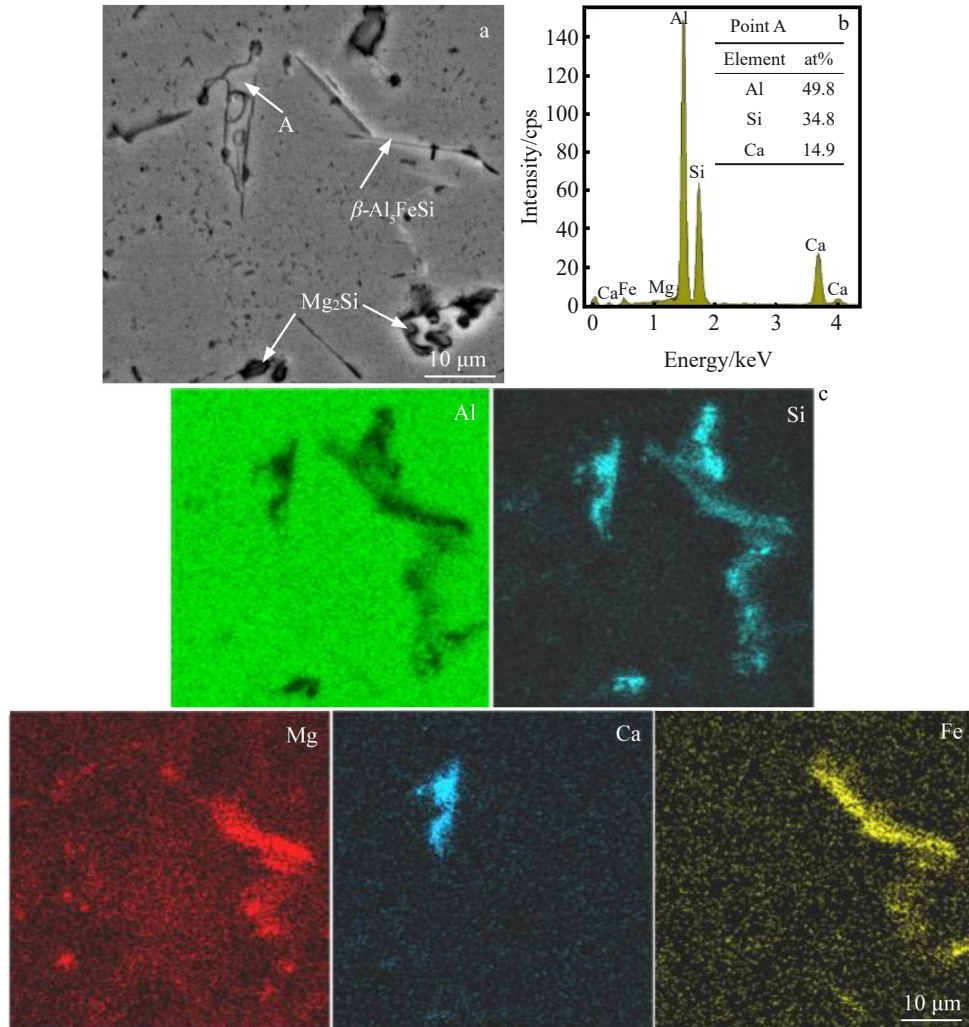


Fig.8 SEM microstructure (a) and corresponding element distributions (c) of AA2# alloy; EDS analysis results of point A in Fig.8a (b)

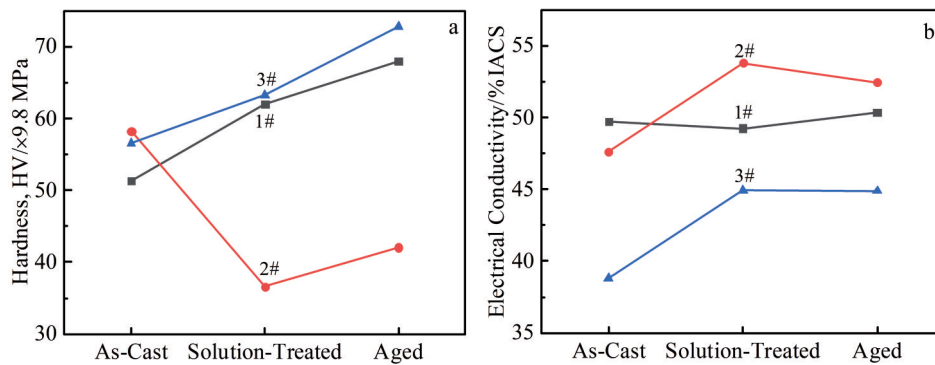


Fig.9 Hardness (a) and electrical conductivity (b) of 1#, 2#, and 3# alloys under different states

solution treatment. These phenomena result in the significantly improved mechanical properties. As shown in Fig.11c and 11d, the as-cast 2# alloy presents the intergranular fracture feature with a few dimples due to the small particle segregation and coarse intermetallic compound particles at the grain boundaries. After aging heat treatment, the AA2# alloy presents the intergranular brittle fracture, which is attributed

to the agglomeration of numerous nanoscale Mg<sub>2</sub>Si and Al<sub>2</sub>Ca particles around the coarse intermetallic compound particles at the grain boundaries, which severely deteriorates the intergranular bonding of  $\alpha$ -Al matrix and results in a sharp decline in mechanical properties of AA2# alloy. The as-cast 3# alloy presents the intergranular brittle fracture due to the particle cracking and small particle segregation at the grain

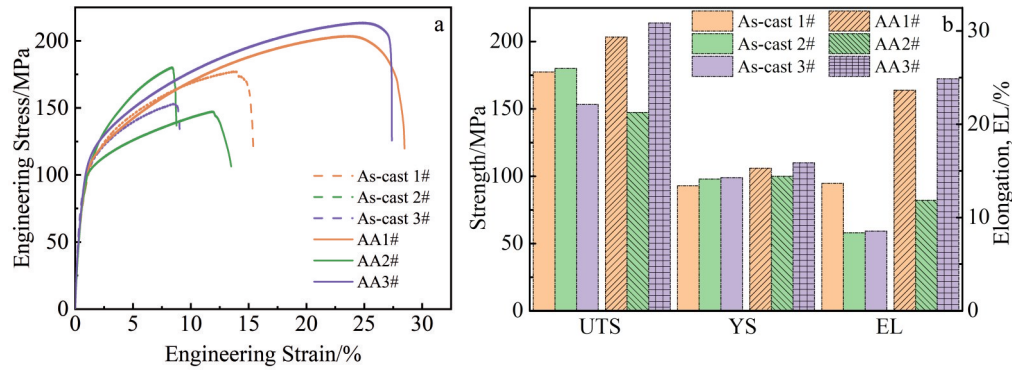


Fig.10 Engineering stress-engineering strain curves (a) and tensile properties (b) of 1#, 2#, and 3# alloys under different states

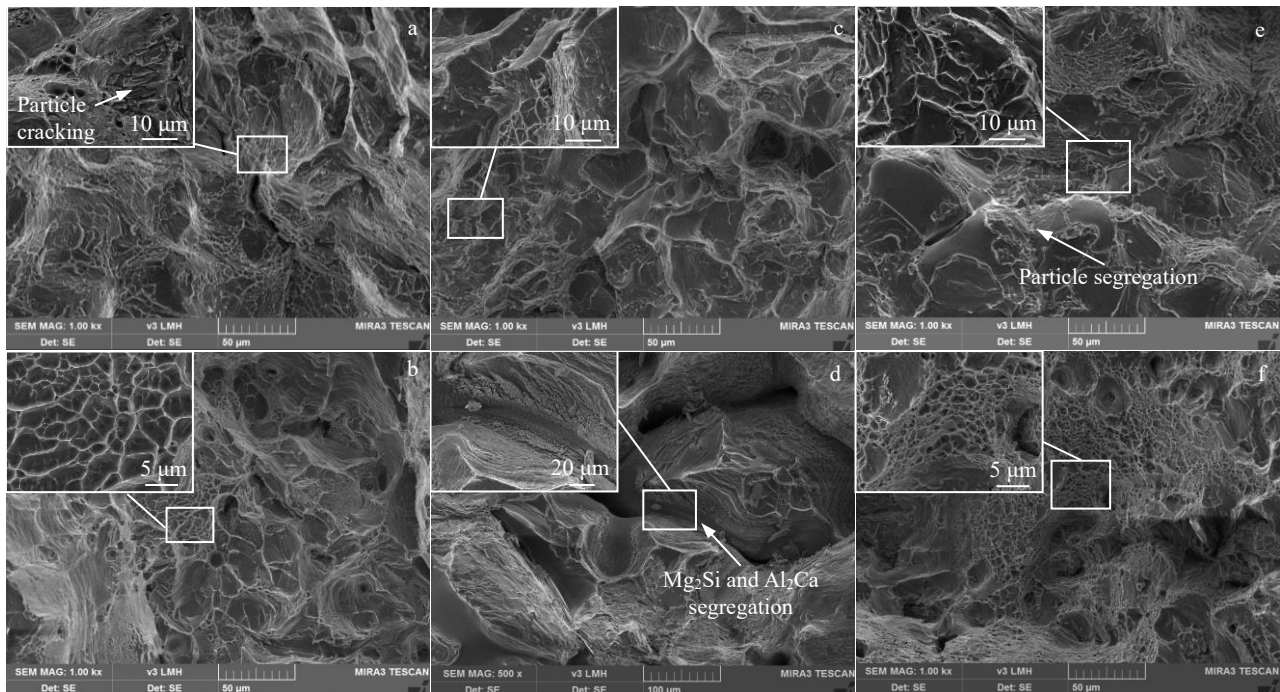


Fig.11 SEM fractographies of as-cast 1# alloy (a), as-cast 2# alloy (c), as-cast 3# alloy (e), AA1# alloy (b), AA2# alloy (d), and AA3# alloy (f)

boundaries. However, the AA3# alloy exhibits the ductile fracture feature. There are a large number of fine dimples on the fracture surface, which results from the dissolution of many coarse intermetallic compound particles and the homogeneous re-precipitation of fine precipitates after the solid solution and aging treatment, which is consistent with the enhanced mechanical properties of AA3# alloy.

### 3 Discussion

#### 3.1 Effect of alloying elements on microstructure

According to the abovementioned results, it can be concluded that the minor Ca addition exerts a significant effect on the grain refinement and  $Mg_2Si$  precipitation in the Al-Mg-Si alloys. In this research, the Ca and Mg exist as the Mg-Al-Si eutectic master alloy, which has fine structure and relatively uniform distribution of the eutectic compound

particles, such as  $(Mg, Al)_2Ca$  and  $Mg_2Ca$ . Thus, numerous fine  $Al_2Ca$  particles form in the aluminum melt during the solidification process, the nucleation occurs, and the uniform distribution of a large number of  $Mg_2Si$  particles in the cast ingot can be observed. Kim et al.<sup>[20]</sup> proved that the Ca and Si in the Al-Mg-Si melt can form the  $CaSi_2$  particles as the nuclei of  $Mg_2Si$  precipitates to promote the  $Mg_2Si$  precipitation. The coarse  $CaSi_2$  compound particle can be observed at the grain boundaries of AA2# alloy, which is consistent with the results in Ref. [20]. Moreover, the heterogeneous nucleation effect of these compound particles plays a great role in the primary  $\alpha-Al$  grain refinement. Nevertheless, Ca has no obvious effect on the  $\beta-Al_3FeSi$  impurity phase. Some particles are pushed to the grain boundaries and a few coarse  $CaSi_2$  compound phases form at the grain boundaries, which is detrimental to the mechanical properties of alloys. After the solid solution and aging treatments, the coarse  $\beta-Al_3FeSi$  impurity phase can

hardly dissolve, and the severe segregation of fine  $Mg_2Si$  and  $Al_2Ca$  particles aggravates the degradation of mechanical properties of AA2# alloy.

Similarly, Mn has the effect of heterogeneous nucleation, which is attributed to the formation of  $Al_6Mn$  particles during the solidification process, thereby refining the matrix grains. Besides, the Mn addition can form  $\alpha-Al(FeMn)Si$  phase, therefore eliminating the Fe impurity in the Al alloys. The  $\alpha-Al(FeMn)Si$  particles dissolve in the matrix through the subsequent solid solution treatment and the residual fine particles can impede the growth of  $\alpha-Al$  grain, thus maintaining the fine-grain structure of ST3# alloy. Moreover, the precipitation of considerable fine particles is promoted after aging treatment.

### 3.2 Effect of microstructure on mechanical properties

The hardness ( $H$ ) of the Al-Mg-Si- $X$  alloys<sup>[21]</sup> can be expressed as follows:

$$H=H_0+H_{gb}+H_p+H_{ss}+H_d \quad (1)$$

where  $H_0$  is the base hardness of the pure Al;  $H_{gb}$ ,  $H_p$ ,  $H_{ss}$ , and  $H_d$  are the hardness contributed by the grain refinement strengthening, precipitation hardening, solid solution hardening, and dislocation hardening, respectively. Among them, the precipitation hardening effect is assumed to be the major influence factor on the hardness<sup>[22]</sup>. The addition of Ca or Mn induces more fine precipitates, resulting in the fact that the hardness of as-cast 2# and 3# alloys is higher than that of as-cast 1# alloy. In addition, the hardness and strength of the as-cast 2# alloy are the highest because the grain size of 2# alloy is the finest and the number of  $Mg_2Si$  precipitates is the largest in 2# alloy. However, the inhomogeneous distribution of the particles around the grain boundaries leads to the lowest UTS of as-cast 3# alloy. While YS of as-cast 3# alloy is slightly improved, compared with that of the as-cast 1# alloy due to the grain refinement.

After the solid solution and aging treatments, the solid solution strengthening and precipitate hardening effects increase the hardness of 1# alloy continuously. Less  $Mg_2Si$  precipitates exist in the AA3# alloy and the inhomogeneous distribution leads to the relatively inferior mechanical properties, compared with those of AA1# alloy. The dispersion hardening caused by the  $Al_6Mn$  and  $\alpha-Al(FeMn)Si$  particles and the precipitation hardening caused by the  $Mg_2Si$

phase both greatly contribute to the high hardness of ST3# and AA3# alloys. The uniform microstructure with a large number of fine and uniformly dispersed precipitates and the elimination effect of  $\alpha-Al(FeMn)Si$  phase jointly result in the optimal mechanical properties of AA3# alloy. The coarsening and agglomeration of  $Mg_2Si$ ,  $Al_2Ca$ , and  $CaSi_2$  particles around the coarse  $\beta-Al_3FeSi$  compound particles at the grain boundaries cause the sharp decline of hardness of ST2# alloy. The hardness of AA2# alloy slightly is increased due to the precipitation of a small number of  $Mg_2Si$  particles. Similarly, the mechanical properties of AA2# alloy are decreased due to the grain boundary weakening.

### 3.3 Effect of microstructure on electrical conductivity

According to the Mattiessen's rule, the total electrical resistivity of Al-Mg-Si- $X$  alloys<sup>[23]</sup> can be expressed by Eq. (2), as follows:

$$\rho_{total}=\rho_0+\rho_{ss}+\rho_d+\rho_{gb}+\rho_p \quad (2)$$

where  $\rho_{total}$  is the total electrical resistivity of the alloy;  $\rho_0$  is the intrinsic electrical resistivity of the lattice;  $\rho_{ss}$ ,  $\rho_d$ ,  $\rho_{gb}$ , and  $\rho_p$  are the electrical resistivity caused by Mg, Si, and Mn solute atoms dissolving in the Al matrix, dislocations, grain boundaries, and precipitates, respectively. In this research, the electrical resistivity of the alloys is mainly affected by the content of solute atoms and the precipitates. The alloying elements dissolving in the Al matrix decrease the electrical conductivity of Al alloys<sup>[13]</sup>. Table 2 summarizes the maximum solubility of several alloying elements in aluminum matrix and the average increment of electrical resistivity for every increase of 1wt% element in/out of solution.

Mg, Si, and Fe elements in the as-cast 1# alloy after solid solution dissolve into the Al matrix, which decreases the electrical conductivity. While the  $Mg_2Si$  precipitation during aging treatment leads to the decrease of  $\rho_{ss}$  by the purification of the matrix. Thus, the electrical conductivity of 1# alloy decreases after solid solution treatment and then increases after aging treatment. It is generally believed that the precipitation can increase the electrical conductivity of Al alloys because the detrimental effect of precipitates on electrical conductivity is less obvious than that of the solid solutes<sup>[24]</sup>, i. e., the precipitations increase the electrical conductivity.

Compared with the as-cast 1# alloy, the Ca addition induces

**Table 2** Maximum solubility of alloying elements in aluminum matrix and the average increment of electrical resistivity for every increase of 1wt% element in/out of solution

Element	Maximum solubility in aluminum matrix/%	Average increment in electrical resistivity for every increase of 1wt% element/ $\mu\Omega \cdot cm$	
		In solution	Out of solution
Mg	14.900	0.54	0.220
Si	1.650	1.02	0.088
Mn	1.820	2.94	0.340
Fe	0.052	2.56	0.058

the Mg<sub>2</sub>Si, CaSi<sub>2</sub>, and Al<sub>2</sub>Ca precipitates of high content, which leads to the decrease of Mg and Si solute atoms in Al matrix, therefore reducing the  $\rho_{ss}$  of as-cast 2# alloy. The precipitates with a dense distribution may impair the electrical conductivity. The relationship between the electrical resistivity caused by the precipitates and their spacing<sup>[24]</sup> can be described by Eq.(3), as follows:

$$\rho_p = \frac{12}{L^{1/2}} \quad (3)$$

where the  $L$  is the spacing of the precipitates.

Therefore, the electrical conductivity of the as-cast 2# alloy is slightly lower than that of as-cast 1# alloy due to the reduced dispersion degree of precipitates in 2# alloy. After the solution treatment, the spacing of precipitates ( $L$ ) in 2# alloy is increased and  $\rho_p$  is decreased due to the coarsening, dissolution, and agglomeration of Mg<sub>2</sub>Si precipitates at the grain boundaries. Although the dissolution of a small number of Mg<sub>2</sub>Si precipitates slightly increases  $\rho_{ss}$ , the decrease in  $\rho_p$  is greater than the increase in  $\rho_{ss}$ , resulting in the highest electrical conductivity of ST2# alloy.

The electrical conductivity of as-cast 3# alloy is the lowest due to the high solubility of Mn in the Al matrix. After solution treatment, the precipitation of Al<sub>6</sub>Mn and Mg<sub>2</sub>Si particles leads to the purification of the matrix and thereby the obvious decrease of  $\rho_{ss}$  in ST3# alloy, although partial  $\alpha$ -Al(FeMn)Si particles dissolve which should slightly increase the  $\rho_{ss}$ . After the aging treatment, more Mg<sub>2</sub>Si particles are precipitated, leading to the purification of matrix. However, the spacing of precipitates is decreased due to the reduced dispersion degree of Mg<sub>2</sub>Si precipitates. The decrease of  $\rho_{ss}$  cannot compensate the increase of  $\rho_p$ . Thus, the electrical conductivity of AA2# and AA3# alloys decreases slightly.

## 4 Conclusions

1) The minor Ca addition has a significant effect on the grain refinement and particle precipitation in the Al-0.59Mg-0.54Si alloy, which leads to the optimal tensile strength of 180 MPa and relatively low electrical conductivity of 47.62%IACS in the as-cast state. The solid solution and aging treatments cause the particle coarsening and agglomeration at the grain boundaries, which contributes to the optimal electrical conductivity of 53.78%IACS of Al-0.59Mg-0.54Si-0.253Ca alloy after solid solution treatment. However, the mechanical properties of Al-0.59Mg-0.54Si-0.253Ca alloy after solid solution and aging treatments are decreased.

2) The minor Mn addition also plays a great role in the grain refinement, particle precipitation, and the elimination of  $\beta$ -Al<sub>5</sub>FeSi impurity phase by the formation of  $\alpha$ -Al(FeMn)Si phase in Al-0.59Mg-0.54Si alloy. The dissolution of  $\alpha$ -Al(FeMn)Si phase and the precipitation of numerous fine particles during the solid solution and aging treatments result in the fine uniform microstructure of Al-0.59Mg-0.54Si-0.253Mn alloy. Therefore, the optimal mechanical properties (ultimate tensile strength of 214 MPa and elongation of 24.9%) and an acceptable electrical conductivity of

44.89%IACS are obtained. The research provides guidance for the design of Al alloy castings with high strength and high electrical conductivity.

## References

- 1 Miller W S, Zhuang L, Bottema J et al. *Materials Science and Engineering A*[J], 2000, 280(1): 37
- 2 Werinos M, Antrekowitsch H, Ebner T et al. *Materials & Design* [J], 2016, 107: 257
- 3 Cui Li, Guo Mingxing, Peng Xiangyang et al. *Acta Metallurgica Sinica*[J], 2015, 51(3): 289 (in Chinese)
- 4 Chen Zhiguo, Yang Wenling, Wang Shiyong et al. *Rare Metal Materials and Engineering*[J], 2010, 39(8): 1499 (in Chinese)
- 5 Zhang Y L, Wei F, Mao J et al. *Materials Characterization*[J], 2019, 158: 109 963
- 6 Cui X L, Cui H W, Wu Y Y et al. *Journal of Alloys and Compounds*[J], 2019, 788: 1322
- 7 Zhao Q R, Qian Z, Cui X L et al. *Journal of Alloys and Compounds*[J], 2016, 666: 50
- 8 Ninomiya R, Ojiro T, Kubota K. *Acta Metallurgica et Materialia* [J], 1995, 43(2): 669
- 9 Terada M, Sota R, Ishimatsu N et al. *Metallurgical and Materials Transactions A*[J], 2004, 35(9): 3029
- 10 Huang Q Y, Liu Y, Tong M et al. *Vacuum*[J], 2020, 177: 109 356
- 11 Suzuki A, Saddock N D, Jones J W et al. *Acta Materialia*[J], 2005, 53(9): 2823
- 12 Zhang J, Kang S B, Yu H S et al. *Materials & Design*[J], 2011, 32(6): 3566
- 13 Totten G. *ASM Handbook*[M]. Cleveland: ASM International, 2016
- 14 Li Bin, Yang Zhao, Yang Xuyue et al. *Rare Metal Materials and Engineering*[J], 2015, 44(11): 2857 (in Chinese)
- 15 Wu X Y, Zhang H R, Ma Z et al. *Journal of Alloys and Compounds*[J], 2019, 786: 205
- 16 Eisaabadi B G, Davami P, Varahram N et al. *Materials Science and Engineering A*[J], 2013, 565: 278
- 17 Wang Hongbin, Zhang Xinyu, Li Shengli et al. *Rare Metal Materials and Engineering*[J], 2021, 50(1): 129 (in Chinese)
- 18 Belov N A, Akopyan T K, Korotkova N O et al. *Materials Letters*[J], 2021, 300: 130 199
- 19 Suzuki A, Saddock N D, Jones J W et al. *Metallurgical and Materials Transactions A*[J], 2006, 37(3): 975
- 20 Kim J J, Kim D H, Shin K S et al. *Scripta Materialia*[J], 1999, 41(3): 333
- 21 Chen Y, Gao N, Sha G et al. *Acta Materialia*[J], 2016, 109: 202
- 22 Kemsies R H, Milkereit B, Wenner S et al. *Materials & Design* [J], 2018, 146: 96
- 23 Han Y, Shao D, Chen B A et al. *Journal of Materials Science*[J], 2017, 52(8): 4445
- 24 Raesinia B, Poole W J, Lloyd D J. *Materials Science and Engineering A*[J], 2006, 420(1): 245

## Ca和Mn添加对铸态及热处理态Al-Mg-Si合金的微观组织、力学性能和导电性能影响

郑毅<sup>1</sup>, 边丽萍<sup>1,2,3</sup>, 冀宏亮<sup>1</sup>, 刘先文<sup>1</sup>, 田丰<sup>1</sup>

(1. 太原理工大学 材料科学与工程学院, 山西 太原 030024)

(2. 太原理工大学 先进镁基材料山西省重点实验室, 山西 太原 030024)

(3. 太原理工大学 先进金属复合材料成形技术与装备教育部工程研究中心, 山西 太原 030024)

**摘要:** 制备了Al-0.59Mg-0.54Si-X (X=0, 0.253Ca, 0.253Mn)合金来探究微量Ca、Mn添加对铸态、固溶态及时效态Al-0.59Mg-0.54Si-X合金的微观组织、力学性能及导电性能的影响。研究发现, Ca和Mn添加都显著细化了 $\alpha$ -Al的晶粒尺寸。Ca能够诱导高密度的Mg<sub>2</sub>Si和Al<sub>2</sub>Ca颗粒在铸态 $\alpha$ -Al晶粒中析出, 使合金在铸态下具有最优的力学性能。固溶和时效处理会导致颗粒粗化并且偏聚在晶界, 使合金的力学性能急剧下降, 但其电导率却增加到了52.44%IACS。Mn添加使得晶界上的粗大 $\beta$ -Al<sub>3</sub>FeSi杂质相转化成 $\alpha$ -Al(FeMn)Si颗粒, 并且诱导Mg<sub>2</sub>Si和AlMn颗粒在铸态合金中析出。因此经过固溶和时效处理后的Al-0.59Mg-0.54Si-0.253Mn合金表现出最优的力学性能以及可接受的电导率。

**关键词:** Al-Mg-Si合金; 合金化元素; 力学性能; 导电性能

作者简介: 郑毅, 男, 1995年生, 硕士, 太原理工大学材料科学与工程学院, 山西 太原 030024, E-mail: 1460121856@qq.com